Influence of Microstructure on the Premature Failure of a Second-Intermediate Sendzimir Mill Drive Roll

A. Ray, D. Mukherjee, B. Sarkar, and S. Mishra

Although a precise understanding of roll failure genesis is complex, the microstructure of a broken roll can often unravel intrinsic deficiencies in material quality responsible for its failure. This is especially relevant in circumstances when, even under a similar mill-operating environment, the failure involves a particular roll or a specific batch of rolls.

This paper provides a microstructural insight into the cause of premature breakage of a second-intermediate Sendzimir mill drive roll used at a stainless steel sheet rolling plant under the Steel Authority of India Limited. Microstructural issues influencing roll quality, such as characteristics of carbides, tempered martensite, retained austenite, etc., have been extensively studied through optical and scanning electron microscopy, electron-probe microanalysis, image analysis, and x-ray diffractometry. These are discussed to elucidate specific microstructural inadequacies that accentuated the failure.

The study reveals that even though retained austenite content is low (6.29 vol%) and martensite is non-acicular, the roll breakage is a consequence of intergranular cracking caused by improper carbide morphology and distribution.

Keywords

carbide segregation, roll failure, Sendzimir mill roll, spalling, tempered martensite

1. Introduction

STEEL rolls for cold reducing mills may fail in different ways depending upon their quality, type, and service conditions undergone. Consequently, their useful life often is limited by roll discard at higher diameters because of gradual loss of hardness and wear resistance, or it is grossly reduced following premature failures. While failures of the former kind are progressive in nature, catastrophic failures by mechanisms, such as cracking and spalling, considerably reduce roll life. Thus, in today's context of high mill productivity and overall roll shop efficiency, the metallurgical requirements of high-quality rolls have assumed great significance.

A precise understanding of the genesis of roll failures is however complex. Inadequate metallurgical quality, improper or abusive mill-usage practices, and abnormal mill operating conditions can singly, or in combination, lead to service failures (Ref 1). Although in actual practice, the majority of such failures usually can be attributed to the aforesaid mill-related factors, the microstructure of a prematurely failed roll can often unravel intrinsic deficiencies in material quality (Ref 2), possibly responsible for the failure. This is especially relevant in circumstances when, even under a similar mill-operating environment, the failure involves a particular roll or a specific batch of rolls.

This paper discusses the microstructural characteristics of a prematurely failed second-intermediate Sendzimir mill drive roll used at a stainless steel strip/sheet rolling plant under the Steel Authority of India Limited. Microstructural issues critical to roll performance, such as the type, content, morphology and distribution of carbides, amount of retained austenite, nature of the martensitic matrix, etc., are elucidated to identify specific microstructural inadequacies that accentuated the roll failure.

A. Ray, D. Mukherjee, B. Sarkar, and **S. Mishra,** Physical Metallurgy Group, Research & Development Centre for Iron & Steel, Steel Authority of India Limited, Ranchi—834 002, India

2. Roll Particulars

2.1 *Roll Arrangement*

The arrangement of various rolls in the 20 roll cluster 1-2-3-4 type Sendzimir mill is schematically depicted in Fig. 1. The small hard work rolls are located between two supporting first-intermediate rolls, which are again supported by six second-intermediate rolls (3 in top and 3 in bottom cluster). The bearing shafts, marked *A* through *H*, have concentrically mounted

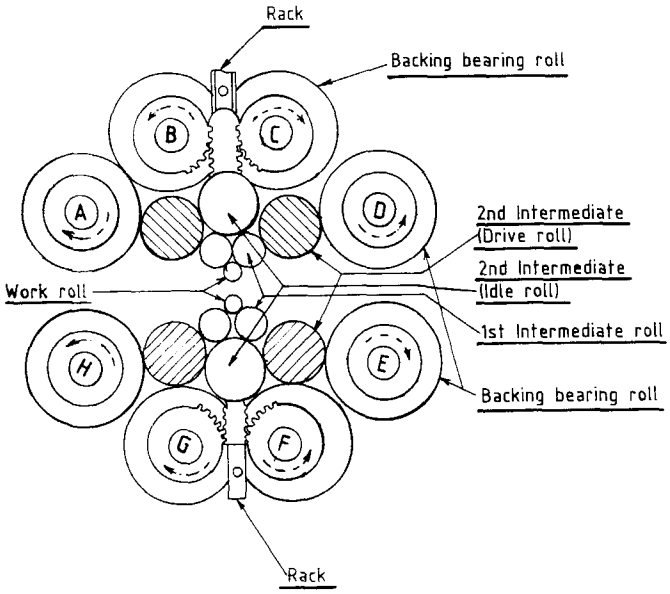

Fig. 1 Schematic arrangement of rolls in the 1-2-3-4 type Sendzimir mill

roller bearings and are located between saddles. The four second-intermediate drive rolls (shown hatched) are power driven through large diameter spindles, which are designed to carry high torque drive at high speeds.

The smaller diameter work rolls, which deform the steel sheets, are driven by the four second-intermediate drive rolls through frictional contact with the first-intermediate rolls. The screw-down mechanism of the mill is regulated by rotary positioning of the two central shafts *B* and *C* by hydraulically driven racks, which engage with the pinions mounted at the shaft ends. The two central shafts *F* and *G*, located below, are used to control the work roll gap by adjusting the lower work roll. The outer shafts *A* and *H*, and *D* and *E*, can be adjusted in pairs to maintain a uniform roll gap for compensating work roll wear.

2.2 *Roll Material*

The 174 mm diam, second-intermediate drive rolls used in this particular Sendzimir mill are made of a 5% Cr-base alloy steel—0.30 to 0.55 wt% C, 1.20 wt% (max) Si, 0.60 wt% (max) Mn, 4.50 to 5.50 wt% Cr, 1.80 wt% (max) Mo, 0.80 wt% (max) V, and 1.80 wt% (max) W.

These rolls are supplied in a forged and hardened condition with a specified surface hardness in the range of 72 to 82° shore C (50.5 to 56.3 HRC).

3. Metallurgical Investigation

Fragmented samples from the broken roll were extensively studied from the standpoint of visual appearance, fracture topography, and microstructural characteristics to identify specific inadequacies in roll quality.

Optical microscopic examinations were carried out at 500× on both etched and unetched polished microsections of the broken roll samples. The polished samples were etched with Villela's reagent (4 g picric acid, 100 mL ethanol, 5 mL hydrochloric acid) for observing the general microstructure comprising alloy carbides, tempered martensite, and retained austenite. Vickers microhardness measurements were carried out parallel with a pneumatic-type LEITZ-MM6 model, Leica, GmbH, Wetzla, Germany, microhardness tester to corroborate phase identification. Unetched specimens were also examined to observe nonmetallic inclusions.

Automatic quantitative image analysis was carried out on polished and etched microsections to determine the volume percent of alloy carbides dispersed in the tempered martensite. The sample was traversed over twenty random fields, and carbide volume fraction in each field was automatically estimated using proprietary application software. The amount of retained austenite present was, however, determined by x-ray diffractometry (XRD) techniques because this phase was not optically discernible in the microstructures subjected to image analysis.

Morphological observations of fracture surfaces were carried out with a scanning electron microscope (SEM), while microstructures of polished and etched specimens were also examined at higher magnifications to discern the extremely fine carbides not observable in optical microscopy. For rapid identification of the chemical constituents in the various carbide species present, qualitative energy dispersive spectrometric (EDS) analysis was carried out in the SEM at 20 kV accelerating voltage and 1×10^{-9} A probe current, using proprietary application software. Quantitative wave-length dispersive (WDS) microanalysis was also carried out on different types of carbides in an electron probe microanalyzer (EPMA) to ascertain their chemistries and to derive their formulas (MC, M_7C_3, etc.) from the atomic percent data. The EPMA analyses were carried out at 15 kV accelerating voltage and 5×10^{-8} A probe current, using proprietary application software.

4. Results and Discussion

4.1 *Roll Chemistry and Hardness*

The composition of the failed 5% Cr-base, alloy steel second-intermediate drive roll is similar to that of a hot-work tool steel of the H13 type (Ref 3). Unlike Sendzimir mill work rolls, which are usually made from high carbon-high chromium varieties of D2 (1.25 wt% C, 12 wt% Cr) or D4 (2.25 wt% C, 12 wt% Cr) type cold-work tool steels (Ref 4) or of tungsten carbide (Ref 5), second-intermediate roll steel composition is leaner in carbon content for enhanced toughness. It has been reported (Ref 6) that toughness for intermediate rolls is more important than wear resistance because the driven second-intermediate rolls have to withstand substantial shear stresses in service. Thus, unlike work-rolls, which normally possess surface hardnesses around 64 HRC, the lower surface hardness range (72 to 82° shore C is equivalent to 50.5 to 56.3 HRC) of the second-intermediate drive roll is commensurate with toughness requirements. The bulk hardness of the failed roll was found to be 56 HRC, which is within specified limits.

4.2 *Fracture Characteristics*

The photograph of a typical fragmented portion of the broken second-intermediate drive roll is shown in Fig. 2. Macroscopic appearance of the fracture surface at the broken end was found to exhibit beach marks typical of spalling. Visually, the texture of the fracture surface showed a porcelain-like lusterless appearance, usually characteristic of high-speed steel (Ref 7). A linear crack is observed running across the spalled area on to the working surface of the roll (Fig. 2). It is, however, not possible to exactly opine whether this crack propagated from the roll interior to the outer roll surface or vice versa.

Morphological observations of fracture specimens in the SEM revealed brittle intergranular failure. The SEM micrograph of a typical spalled area exhibiting intergranular cracking is shown in Fig. 3 at 1000×. This suggests that spalling in this roll is a consequence of intergranular cracking, whose initiation and propagation presumably has been aided by imposed stresses during rolling.

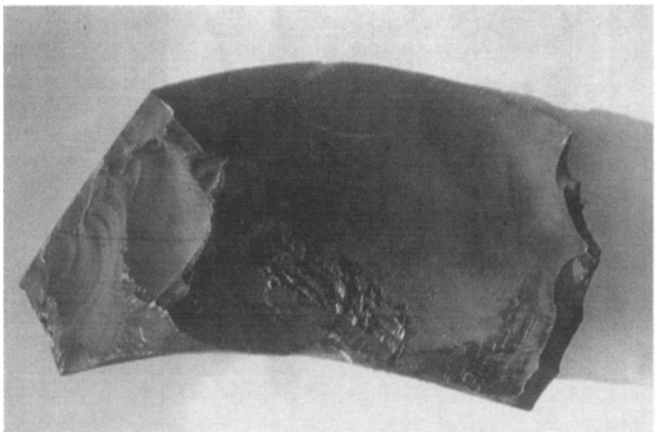

Fig. 2 Macroscopic appearance of broken roll piece showing spalling

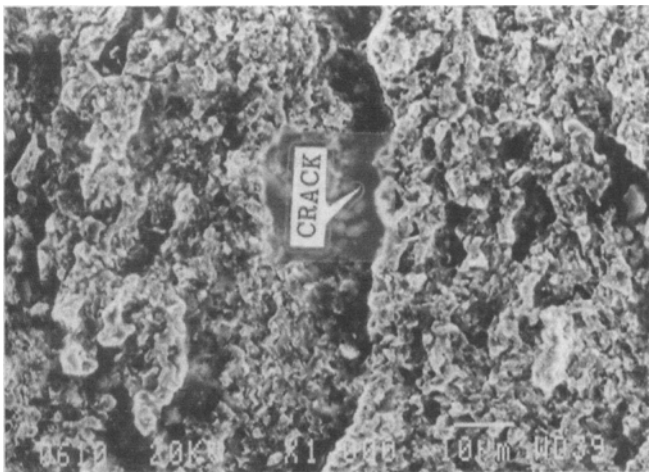

Fig. 3 SEM fractograph of spalled surface showing brittle intergranular cracking. 1000×

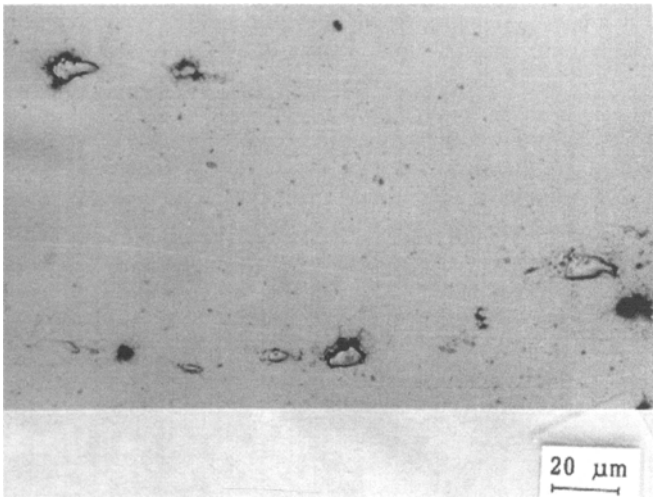

Fig. 4 Unetched roll microstructure showing random distribution of small and isolated V-rich carbide particles. 500×

4.3 *Microstructure and Carbide Distribution*

Optical microscopic observations of polished and unetched specimens at 500× revealed that the sample was clean from the standpoint of nonmetallic inclusions and was virtually free from harmful oxide and nitride-type inclusions. However, a number of randomly distributed small and isolated particles (subsequently confirmed by EPMA analyses as V-rich alloy carbides) with light-pinkish tinge were observed (Fig. 4) in the unetched state. The Villela-etched microstructure of the broken roll samples revealed massive carbide segregated networks at many places, along with dispersions of extremely fine globular carbides in a matrix of dark-etching tempered martensite (Fig. 5). The tempered martensitic matrix, being nonacicular, reflects a low level of internal stress and is, therefore, unlikely to accentuate failure. Retained austenite was, however, not optically discernible in the microstructures observed at 500×, presumably because of its low content. Typical micrographs showing inhomogeneity of carbide distribution in the broken roll are shown in Fig. 5(a) and (b) at 500×. It is clearly evident from Fig. 5(a) that the carbide segregations have occurred preferentially along grain boundary contours. The massive carbide network depicted in Fig. 5(b) reveals a skeleton-like morphology, presumably indicative of its eutectic origin, i.e., genesis at the ingot solidification stage. The extremely fine globular carbides dispersed elsewhere are apparently of secondary nature; i.e., precipitated during heat treatment of the roll at the manufacturing stage. The preponderance of carbide segregations along grain boundaries also may suggest inadequate deformation imparted at the forging stage of roll manufacture.

The microhardness of the carbide-segregated zones was ~1220 VPN, while the isolated particles of V-rich alloy carbides (Fig. 4) were much harder with a microhardness as high as 1800 VPN. Although carbide segregated zones and the finely dispersed globular carbides were not visible in the unetched condition, the revelation of the V-rich alloy carbides can be attributed to the microrelief of these hard (1800 VPN) particles vis-a-vis the tempered martensite matrix and all the other carbide species present.

The presence of carbides as massive segregated networks, rather than in finely dispersed globular morphology, is extremely detrimental to strength, toughness, fatigue strength, and contact endurance of steels (Ref 8). Because contact-fatigue strength (Ref 9) is an important roll property that influences its spalling propensity, a uniform carbide distribution is all the more desirable. This is because finely dispersed carbides, by virtue of their better cohesion with the matrix, not only enhance wear resistance, but also inhibit microcracking (Ref 10) on the roll skin, as can be caused by shear stresses, which occur in rolling. Figure 6 shows the optical micrograph of a fine crack running through a carbide segregated area. This lends credence to the fact that microcracking in this failed roll was aided by the presence of carbide segregations.

4.4 *Carbide and Retained Austenite Contents*

The average volume fraction of alloy carbides determined by automatic image analysis measurements on Villela-etched

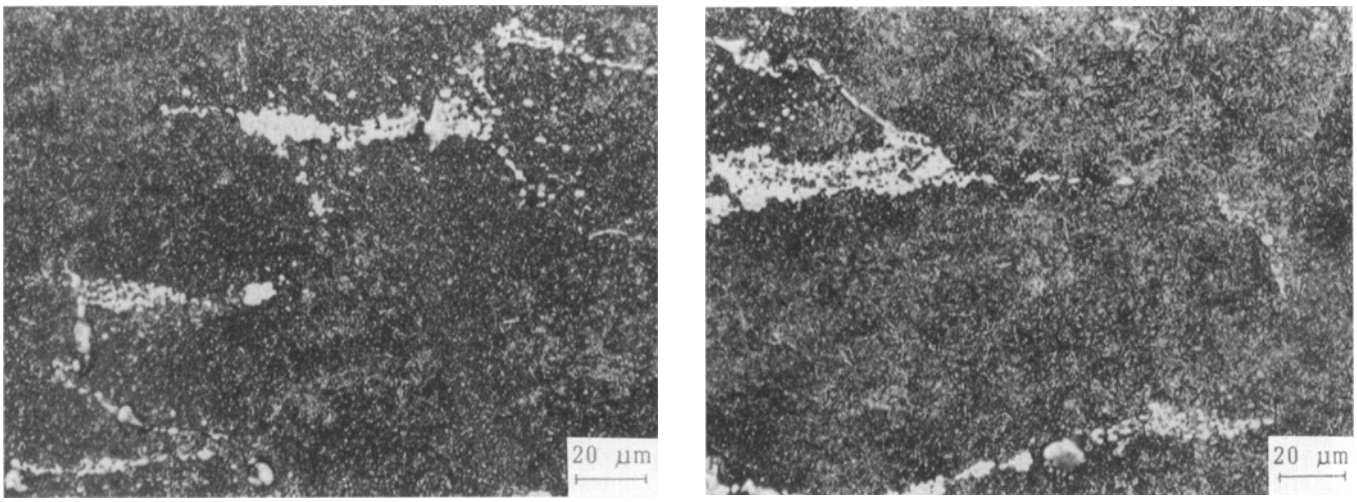

(a) (b)

Fig. 5 Villela-etched roll microstructure showing inhomogeneous carbide distribution in tempered martensite. (a) Carbide segregation at grain boundaries. (b) Massive carbide segregate with skeleton-like appearance. 500×

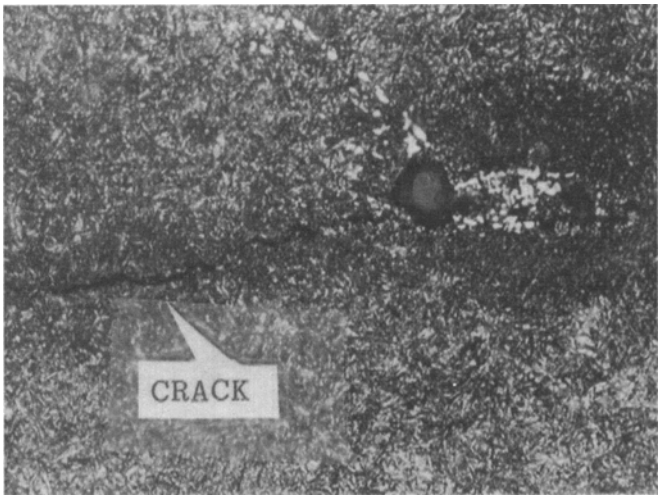

Fig. 6 Villela-etched roll microstructure showing microcracking across segregated carbide. Matrix is tempered martensite. 500×

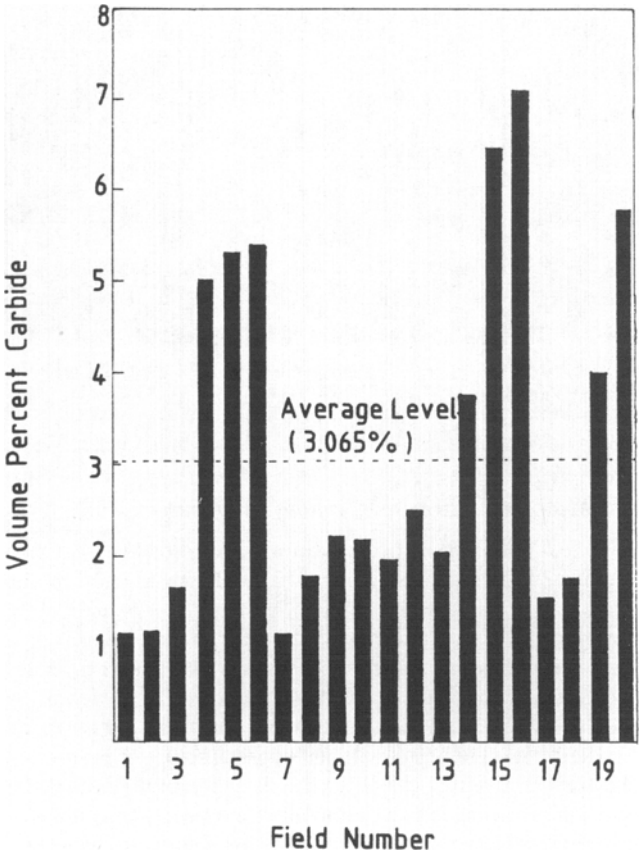

Fig. 7 Histogram plot showing field-wise variation in carbide volume fraction in failed roll

microsections was 3.065%. The field-wise variation of carbide content (vol%) depicted in Fig. 7 as a histogram plot shows gross inhomogeneity in carbide distribution with values ranging from 1 to 7 vol%. The fields displaying tall bars pertain to pockets of carbide segregated zones where the carbide vol% is significantly higher than the aforesaid average value. However, the average vol% data of carbides is slightly underestimated because some of the extremely fine globular carbides (which were discernible in the SEM at magnifications over 2000×) were not detectable in the optical microstructure subjected to image analysis. It was reported (Ref 11) that H13 type hot-work steel, which possesses similar carbon content and alloy chemistry to that of the failed roll, contains ~3.5% carbides in the annealed state. The average volume fraction of carbides in the failed roll, as determined by image analysis, is therefore not grossly out of place. Because retained austenite was not discernible in optical microscopic images, its content was determined by XRD techniques rather than by image analysis. The

Table 1 Quantitative electron probe microanalysis of MC-type vanadium-rich carbide in roll sample

Element	Conc, %	Atom %	K, %	ZAF	Z	A	F
C	17.698	50.674	6.894	2.5671	0.8169	3.1425	1.0000
Cr	10.682	7.064	10.454	1.0218	1.0085	1.0170	0.9963
V	51.481	34.752	48.962	1.0514	1.0272	1.0259	0.9977
Fe	2.532	1.559	2.374	1.0665	1.0075	1.0612	0.9976
W	11.158	2.087	8.221	1.3572	1.3521	1.0037	1.0000
Mo	10.784	3.865	9.161	1.1772	1.0951	1.0783	0.9969
	104.334	100.000	86.066	(PAC1)	(PH-TX)		

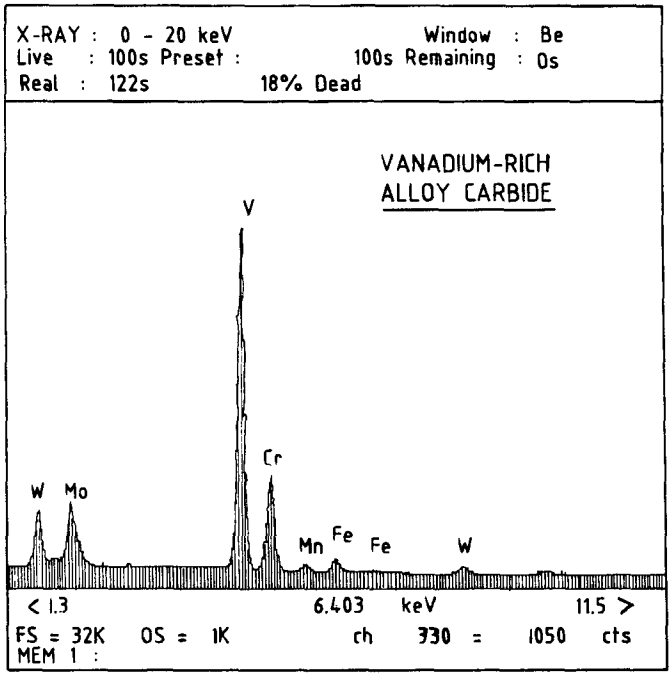

Fig. 8 EDS spectrum of vanadium-rich alloy carbide

amount of retained austenite determined through XRD using Mo-Kα radiation was 6.29%. The low retained austenite content obtained is not indicative of overheating during the hardening stage of roll manufacture. Investigations have reported (Ref 12) that a low retained austenite content (between 5 and 10%) is preferable for minimizing spalling propensity. The retained austenite level (6.29%) in the failed roll thus can be considered normal from the standpoint of roll quality.

4.5 *Carbide Chemistry*

Microscopic observations of broken roll specimens revealed three different types of carbides: randomly distributed small and isolated carbides visible even in the unetched condition (Fig. 4), network-type carbide segregations at grain boundaries, and uniform dispersions of extremely fine globular carbides (Fig. 5). Qualitative EDS analysis in the SEM indicated that the carbides of the first type (small and isolated) were essentially vanadium rich, as depicted in Fig. 8. Quantitative electron probe microanalysis of said carbide as shown in Table 1 indicated a vanadium concentration of 55.697 wt% and a carbon content of 17.672 wt%. The data of carbon (49.689 at.%) show that carbon and the combined metallics are virtually present in equal proportions (~50 at.% each) indicating that the V-rich carbide is of the MC-type. This inference is also corroborated by the extremely high microhardness (1800 VPN) of this carbide.

A series of EPMA micrographs showing improper carbide morphology and distribution in a typical field of the failed roll are shown in Fig. 9 at 2000×. The secondary electron (SE) image in Fig. 9(a) shows a chain-like carbide segregation with a relatively large triangular particle. Numerous fine globular carbides are found dispersed throughout the tempered martensite matrix. The apparent sizes of these fine globular carbides (as can be judged from the micron marker) is much lower than 1 μm (lower than the spatial resolution limit of the EPMA) and are hence not amenable to electron-probe microanalysis. The backscattered electron (BSE) image of the same field shown in Fig. 9(b) reveals compositional contrast based on atomic number differences of the constituent elements in the carbide segregate. The elemental x-ray dot-mapping images of Cr, V, Mo, W, Fe, and C are shown in Fig. 9(c) through (h), respectively. The triangular particle displaying a greyish contrast in the BSE image is essentially V-rich, see Fig. 9(d). The chain-like carbide segregation, which is associated with the triangular V-rich carbide, appears to be essentially Cr-rich, although it does contain varying amounts of V, W, and Mo. The molybdenum and tungsten x-ray mapping images shown in Fig. 9(e) and (f) indicate that the whitish regions of the carbide segregate shown in the BSE image (Fig. 9b), essentially contain W and Mo. The presence of W, which possesses the highest atomic number ($Z = 74$) as compared to all other associated elements in the carbide segregate, is responsible for imparting a white tone in the BSE image. The regions of the segregate associated with lower atomic number elements, such as V ($Z = 23$) and Cr ($Z = 24$), display a greyish contrast in the BSE image. The EDS spectrum of a Cr-rich area in the carbide segregate is shown in Fig. 10, while that of the W-rich regions is shown in Fig. 11. The EDS spectra of these carbides do not reveal carbon because the x-rays emitted from this low atomic number ($Z = 6$) element are beyond the detection capability of the detector. The occurrence of FeKα peaks at 6.403 KeV in Fig. 10 and 11 are due to matrix excitation, possibly caused by small dimensions of the analyzed particles constituting the segregates.

A typical quantitative electron probe microanalysis of the carbide segregation corresponding to the W-rich regions (appearing white in the BSE image) is furnished in Table 2. Unlike the V-rich carbides of the MC-type, the carbon and vanadium contents in this segregated carbide are lower, being 7.647 and 9.293 wt%, respectively. On the contrary, the W and Mo contents in this carbide are also higher, being 23.629 and 21.443

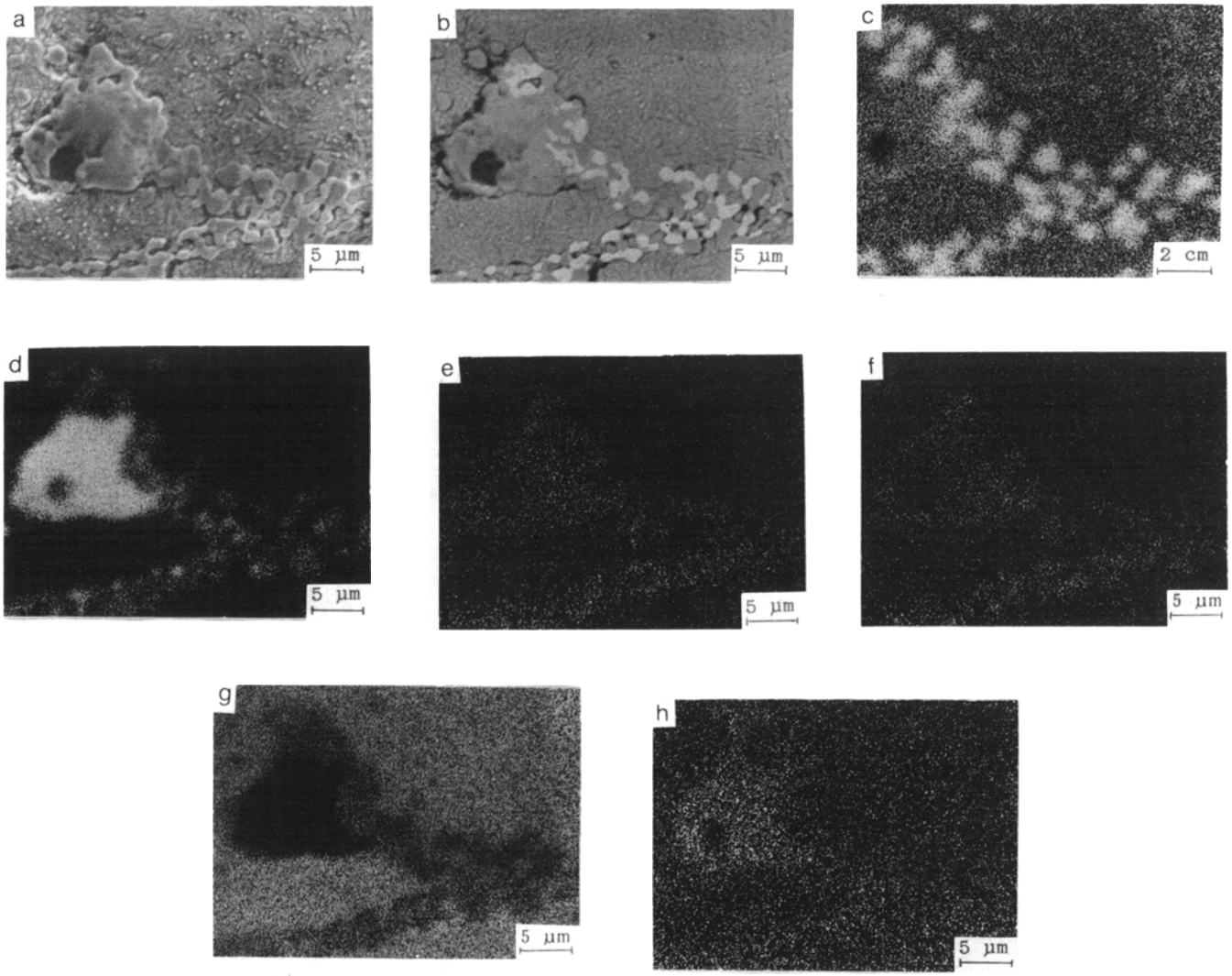

Fig. 9 EPMA micrographs of typical carbide segregation in failed roll. (a) SE image. (b) BSE image showing atomic number contrast. (c) Cr x-ray dot map. (d) V x-ray dot map. (e) Mo x-ray dot map. (f) W x-ray dot map. (g) Fe x-ray dot map. (h) C x-ray dot map. 2000×

Table 2 Quantitative electron probe microanalysis of M_7C_3-type alloy carbide segregate in roll sample

Element	Conc, %	Atom %	K, %	ZAF	Z	A	F
C	7.647	35.696	2.218	3.4479	0.7627	4.5206	1.0000
Cr	5.609	6.048	5.812	0.9651	0.9556	1.0453	0.9662
V	9.293	10.228	9.152	1.0154	0.9747	1.0631	0.9799
Fe	28.187	28.294	28.743	0.9807	0.9513	1.0370	0.9940
W	23.629	7.205	18.627	1.2686	1.2607	1.0063	1.0000
Mo	21.443	12.530	17.191	1.2474	1.0447	1.1949	0.9992
	95.809	100.000	81.743	(PAC1)	(PH-TX)		

wt%, respectively. The data for carbon being 35.696 at.% and that of the combined metallics (Cr + V + Fe + W + Mo) being 64.304 at.%, respectively, indicates that the specific segregated carbide analyzed approximates to the stoichiometric formula M_7C_3. Table 3 shows the quantitative electron probe microanalysis data at another W-rich spot of the segregated carbide. The carbon content at this spot is appreciably lower (4.803 wt%), while the chromium content is marginally higher (7.463 wt%) than that in the spot analysis depicted in Table 2. Table 3 shows that the data for carbon is 22.65 at.%, while that of the combined metallics (Cr + V + Fe + W + Mo) is 77.35 at.%. This

Table 3 Quantitative electron probe microanalysis of $M_{23}C_6$-type alloy carbide segregate in roll sample

Element	Conc, %	Atom %	K, %	ZAF	Z	A	F
C	4.803	22.650	1.580	3.0405	0.7574	4.0144	1.0000
Cr	7.463	8.128	8.085	0.9231	0.9509	1.0369	0.9362
V	3.122	3.470	3.181	0.9814	0.9699	1.0521	0.9617
Fe	49.753	50.452	51.319	0.9695	0.9467	1.0284	0.9958
W	17.404	5.361	13.700	1.2704	1.2556	1.0118	1.0000
Mo	16.834	9.938	13.649	1.2333	1.0395	1.1876	0.9991
	99.379	100.000	91.514	(PAC1)	(PH-TX)		

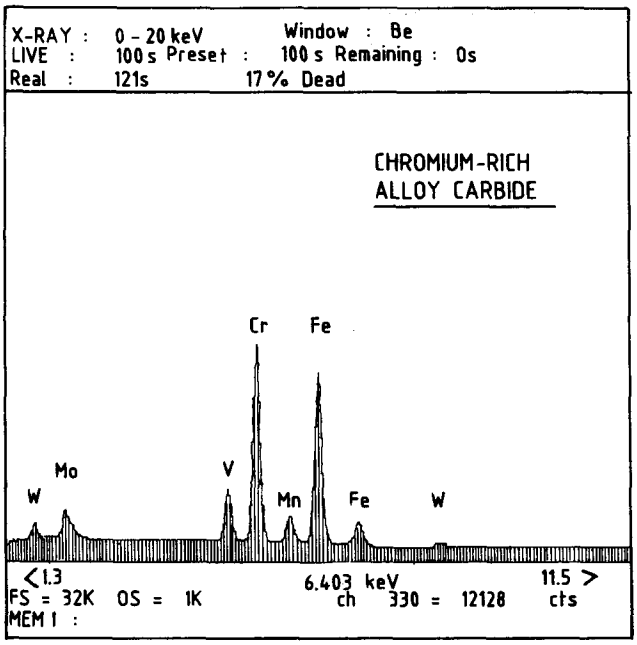

Fig. 10 EDS spectrum of chromium-rich region in alloy carbide segregate

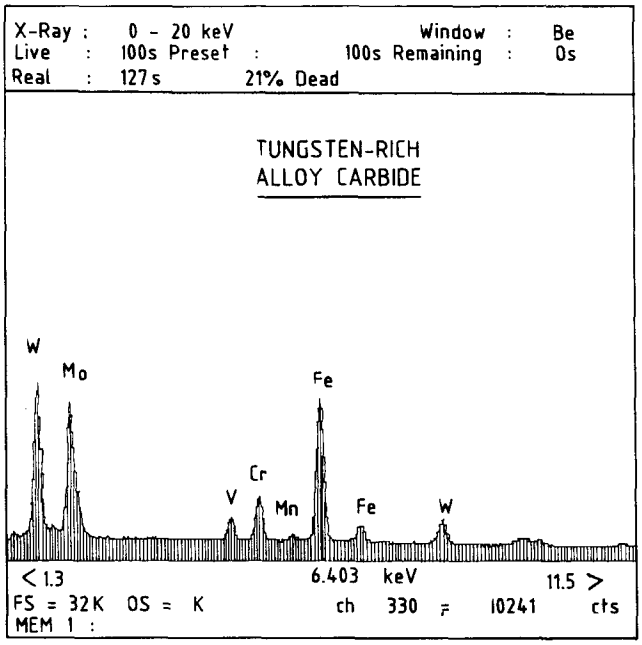

Fig. 11 EDS spectrum of tungsten-rich region in alloy carbide segregate

at.% ratio indicates that the analyzed carbide is of the $M_{23}C_6$ variety.

Electron probe microanalysis of the carbide segregated zones, therefore, indicates the coexistence of both M_7C_3 and $M_{23}C_6$ types of alloy carbides. The presence of significantly higher amounts of tungsten in the carbide segregations, as compared to that in the MC-type isolated carbides, reinforces the fact that carbide inhomogeneity in tool steels is higher in the presence of tungsten (Ref 8).

5. Conclusion

- Although the average carbide content (3.065 vol%) is apparently normal for this grade of steel, field-to-field variations of carbide volume fraction (between 1 and 7%) indicate gross carbide segregations at grain boundaries. The skeleton-like morphology of the massive carbide segregates at grain boundaries presumably indicates their eutectic origin, i.e., genesis at the ingot solidification stage. Their preponderance, even in the finished roll, may indicate inadequate deformation imparted at the forging stage during roll manufacture.
- SEM revelations of brittle intergranular cracking in fracture samples, as well as optical microscopic manifestations of microcracking along carbides, explains the roll of grain boundary carbide segregations in initiating cracks. The premature breakage of the roll is thus a consequence of the propagation of such cracks under applied stresses imposed during rolling.
- Electron probe microanalysis indicated that the randomly distributed isolated carbides, visible even in unetched microsections, were V-rich, MC-type carbides. On the other hand, the complex alloy (Cr-V-W-Mo) carbide segregates were essentially of M_7C_3 and $M_{23}C_6$ types.

  The incidence of large amounts of W (23.6 wt%) in the segregated carbides, as compared to substantially lower W contents (11.15 wt%) in the isolated MC-type, V-rich carbides, corroborates the segregation promoting tendency of W.
- The retained austenite content (6.29%) in the failed roll is low and, being within acceptable limits for forged and hard-

ened steel rolls, is therefore unlikely to aggravate spalling propensity.

- The role of tempered martensite in accentuating spalling is rendered innocuous because the matrix, being nonacicular, reflects a low level of internal stress in the roll.

Acknowledgments

The authors are grateful to Dr. S. Banerjee, Director, Research and Development Centre for Iron and Steel, SAIL for his encouragement and support. Thanks are especially due to Mr. C.B. Sharma and Mr. B.B. Patra for their help in the investigation.

References

1. S.G. Manganello and D.R. Churba, Roll Failures and What to Do When They Occur, *Iron Steelmaker*, Vol 7 (No. 12), 1980, p 26-34
2. D. Mukherjee, A. Ray, and S.K. Bhattacharyya, Spalling Resistance of Forged Steel Cold Rolling Mill Rolls: A Microstructural Insight, *Mater. Forum*, Vol 16 (No. 4), 1992, p 317-325
3. G.A. Roberts and R.A. Cary, Class 520 Chromium-Molybdenum Hot Work Die Steels, *Tool Steels*, American Society for Metals, 1980, p 578-593
4. V.A. Kortesoja, Selection of Material for Rolls for the Metalworking Industry, *Properties and Selection of Tool Materials*, American Society for Metals, 1975, p 254-263
5. A.J. Bill and H.C. Scriven, Sendzimir Mills for Cold Rolling in BSC Stainless, *Flat Rolling A Comparison of Rolling Mill Types*, The Metals Society, 1979, p 163-169
6. M.G. Sendzimir, Sendzimir Mills and their Rolls, *31st Mechanical Working and Steel Processing Conference Proceedings*, Vol XXVII, The Iron and Steel Society, 1990, p 329-334
7. A. Gulayev, High-Speed Steels, *Physical Metallurgy*, Vol 2, Mir Publishers, 1980, p 87-101
8. Y. Geller, Carbide Inhomogeneity, *Tool Steels*, Mir Publishers, 1978, p 197-214
9. M. Nakagawa, A. Hoshi, A. Asano, and Y. Nambu, Causes and Countermeasures of Spalling of Cold Mill Work Rolls, *Iron Steel Eng.*, Vol 58 (No. 3), 1981, p 44-49
10. C. Gaspard, P. Cosse, and A. Magnee, Contribution of ESR and Progressive Induction Hardening to the Manufacture of Deep Hardened Work Rolls, *26th Mechanical Working and Steel Processing Conference Proceedings*, Vol XXII, The Iron and Steel Society, 1985, p 75-87
11. W.F. Smith, Hot-Work Tool Steels, *Structure and Properties of Engineering Alloys*, McGraw-Hill Book Company, 1981, p 382-386
12. W. Patt, Production and Properties of High-Cr-Rolls and Their Behaviour in Cold Strip Mills, *26th Mechanical Working and Steel Processing Conference Proceedings, Vol XXII, The Iron and Steel Society, 1985, p 101-107*